

# A Primal-Dual Interior Point Method for Large-Scale Free Material Optimization

Alemseged Gebrehiwot Weldeyesus\* and Mathias Stolpe†

## Abstract

Free Material Optimization (FMO) is a branch of structural optimization in which the design variable is the elastic material tensor that is allowed to vary over the design domain. The requirements are that the material tensor is symmetric positive semidefinite with bounded trace. The resulting optimization problem is a nonlinear semidefinite program with many small matrix inequalities for which a special-purpose optimization method should be developed. The objective of this article is to propose an efficient primal-dual interior point method for FMO that can robustly and accurately solve large-scale problems. Several equivalent formulations of FMO problems are discussed and recommendations on the best choice based on the results from our numerical experiments are presented. Furthermore, the choice of search direction is also investigated numerically and a recommendation is given. The number of iterations the interior point method requires is modest and increases only marginally with problem size. The computed optimal solutions obtain a higher precision than other available special-purpose methods for FMO. The efficiency and robustness of the method is demonstrated by numerical experiments on a set of large-scale FMO problems.

**Mathematics Subject Classification 2010:** 90C22, 90C90, 74P05, 74P15

**Keywords:** Structural optimization, free material optimization, semidefinite programming, interior point methods

---

\*DTU Wind Energy, Technical University of Denmark, Frederiksborgvej 399, 4000 Roskilde, Denmark. E-mail: alwel@dtu.dk

†DTU Wind Energy, Technical University of Denmark, Frederiksborgvej 399, 4000 Roskilde, Denmark. E-mail: matst@dtu.dk

# 1 Introduction

The fundamental concept of Free Material Optimization (FMO) was introduced in the early 1990s in [6], [7], and [25]. Since then FMO has become one of the growing research areas within structural optimization. In FMO the design variable is the material tensor which can vary at each point of the design domain. Certain necessary conditions on the attainability are the only imposed requirements on the material tensor. The material tensors in FMO are forced to be symmetric positive semidefinite and have bounded trace. FMO thus yields optimal structures by describing not only the distribution of the amount of material but also the local material properties. Therefore, the optimal structure found by FMO can be considered as an ultimately best structure among all possible elastic continua [37]. However, the design is ideal as the manufacturing of structures with, generally anisotropic, material properties changing at each point of the design domain is difficult and expensive. Nevertheless, FMO can be used to generate benchmark solutions with which other models and methods can be compared and to propose novel ideas for new design situations.

The first models in FMO considered finding the stiffest (minimizing static compliance) structure by distributing limited resources of material. There has been significant progress in extending these basic models and multidisciplinary FMO problems have been proposed. FMO problems with constraints on local stresses and displacements are presented and solved in [20], [19], and [15]. FMO problems with constraints on fundamental eigenfrequencies are described and solved in [27]. FMO models for three dimensional structures are developed and analysed in [15] and for plates and shells in [13]. Theoretical aspects including proofs of existence of optimal solutions of FMO problems can be found in e.g. [34].

Due to the conditions imposed on the elasticity tensor in FMO, the resulting optimization problem is a nonlinear semidefinite programming (SDP), a non-standard problem with many matrix inequalities for which special optimization methods have to be developed and implemented. Already in [25] an interior point method was used to solve small size FMO problems. The formulations in [25] have slightly different matrix inequalities compared to recent FMO models. A method based on penalty/barrier multipliers called PBM is used in [37] to solve FMO problems. A computer code PENNON which uses an augmented Lagrangian function method is also developed to solve convex nonlinear and semidefinite programming in [18] and is studied further in [26]. Several FMO problems are solved with this method, for example in [19] and [20]. The focus of today's development of optimization methods for FMO problems is based on first-order methods. Second-order methods are considered computationally too expensive. The most recent methods in [29, 28] are based on a sequential convex

programming concept in which the subproblems are convex and separable SDPs. The approach often leads to large number of iterations but can achieve relatively high accuracy.

The objective of this article is to propose an efficient primal-dual interior point method for the, by now, classical FMO formulations. The method is capable of efficiently and accurately solving large-scale FMO problems. The method and the implementation exploit the property that FMO problems have many but small matrix inequalities. The method computes accurate optimal solution within relatively few iterations. The numerical results indicate that the number of iterations furthermore only increases slowly, if at all, with problem size. The method is developed by extending existing robust and efficient primal-dual interior point method for nonlinear programming and coupling it with existing techniques for linear SDP. The method is also inspired by the developments in interior point methods for general nonlinear SDP problems, see e.g. [35] and [32]. For an overview of primal-dual interior point methods for nonlinear (and non convex) problems, see [11], [12], and [8]. Optimization methods for SDPs are listed in [22] and the references cited therein.

We consider two basic FMO problems which are the primal minimum compliance (maximum overall stiffness) problem and the primal minimum weight problem. For these problems different equivalent linear and nonlinear primal and dual formulations are available. Some of the important mathematical properties of the problems are listed. The primal-dual interior point method is then used to solve problem instances of all stated formulations. It is important that symmetry is maintained in the linearised first-order optimality conditions of SDP problems. There are different symmetrization schemes that are used to maintain the symmetry giving different search directions [30]. The most commonly used directions are the AHO direction [2], the HRVW/KSV/M direction [16, 17, 21], and the NT direction [23, 24]. All of these directions are implemented and a comparison of their computational complexity and effect on numerical convergence is reported.

The outline of this article is as follows. In Section 2 various FMO problem formulations with some of the useful mathematical properties are presented. In Section 3 the general outline of the proposed primal-dual interior point method is described for a generic nonlinear SDP. The algorithmic details of the method specialized to FMO problems are described in Section 4. The implementation of the method and the algorithmic parameters are described in Section 5. In Section 6 the numerical experiments, results and discussion are presented. The conclusions of this paper are given in Section 7.

## 2 FMO problem formulations

We start with the discrete version of the minimum compliance (maximum stiffness) and the minimum weight FMO formulations on two- or three-dimensional design domains. The problem formulations and the finite element discretization are exactly as proposed in published articles on FMO, see e.g. [29] and [20], without any alterations. Existence of optimal solutions to the problem formulations that we consider is shown in [15] under natural assumptions. The design domain  $\Omega$  is partitioned into  $m$  uniform finite elements  $\Omega_i$  for  $i = 1, \dots, m$ . The elastic stiffness tensor  $E(x)$  is approximated by a function that is constant on each finite element. Let the element values constitute the vectors of block matrices  $E = (E_1, \dots, E_m)^T$ . Given the external static nodal load vectors  $f_\ell \in \mathbb{R}^n$  for  $\ell \in L = \{1, \dots, n_L\}$ , where  $n$  is number of (finite element) degrees of freedom, the displacement  $u_\ell$  must satisfy the linear elastic equilibrium equation

$$A(E)u_\ell = f_\ell, \ell \in L \quad (1)$$

where the stiffness matrix  $A(E)$  is given by

$$A(E) = \sum_{i=1}^m A_i(E), \quad A_i(E) = \sum_{k=1}^{n_G} B_{i,k}^T E_i B_{i,k}. \quad (2)$$

The (scaled) strain-displacement matrices  $B_{i,k}$  are appropriately constructed from the derivative of the shape functions and  $n_G$  is the number of Gaussian integration points, see e.g. [9].

The two considered basic FMO formulations are the primal minimum compliance problem

$$\begin{aligned} & \underset{u_1, \dots, u_{n_L} \in \mathbb{R}^n, E \in \mathbb{E}}{\text{minimize}} && \sum_{\ell \in L} w_\ell f_\ell^T u_\ell \\ & \text{subject to} && A(E)u_\ell = f_\ell, \forall \ell \in L, \\ & && \sum_{i=1}^m \text{Tr}(E_i) \leq V, \end{aligned} \quad (3)$$

and the primal minimum weight problem

$$\begin{aligned} & \underset{u_1, \dots, u_{n_L} \in \mathbb{R}^n, E \in \mathbb{E}}{\text{minimize}} && \sum_{i=1}^m \text{Tr}(E_i) \\ & \text{subject to} && A(E)u_\ell = f_\ell, \forall \ell \in L, \\ & && \sum_{\ell=1}^L w_\ell f_\ell^T u_\ell \leq \gamma, \end{aligned} \quad (4)$$

where  $\mathbb{E}$ , denotes the set of admissible materials

$$\mathbb{E} := \{E \in (\mathbb{S}_+^N)^m \mid \underline{\rho} \leq \text{Tr}(E_i) \leq \bar{\rho}, i = 1, \dots, m\}.$$

Here,  $\mathbb{S}_+^N$  is the cone of positive semidefinite matrices in the space  $\mathbb{S}^N$  of symmetric  $N \times N$  matrices. We say that  $E_i \in \mathbb{S}_+^N$  if and only if  $E_i = E_i^T$  and  $E_i \succeq 0$ . The given weights  $w_\ell$  satisfy  $\sum_\ell w_\ell = 1$ , and  $w_\ell > 0$  for each  $\ell \in L$ . For FMO problems on two-dimensional design domains  $N$  takes the value 3. For problems on three dimensional design domains  $N = 6$ . The positive semidefiniteness of  $E$  is a necessary condition on the physically attainability of the material. The  $\text{Tr}(E_i)$  measures the stiffness of the material and is locally bounded from above by  $\bar{\rho}$  to avoid locally arbitrarily stiff material. We also allow a lower trace bounds. Note that  $0 \leq \underline{\rho} < \bar{\rho} < \infty$ . The constant  $V > 0$  is an upper bound on the amount of resource material to distribute in the structure.

Both problems (3) and (4) have linear objective function with linear matrix inequalities and nonlinear (and nonconvex) vector constraints. Therefore, they are classified as nonconvex SDPs.

If we additionally assume that  $E \succ 0^1$  and that, as a consequence, the stiffness matrix  $A(E)$  is positive definite and so non-singular we can obtain a nested problem formulation, i.e. a formulation in the design variables  $E$  only. By solving for the displacement  $u_\ell$  in the equilibrium equation (1), we get the reduced nested formulation of the minimum compliance problem (3)

$$\begin{aligned} & \underset{E \in \mathbb{E}}{\text{minimize}} && \sum_{\ell \in L} w_\ell f_\ell^T A^{-1}(E) f_\ell \\ & \text{subject to} && \sum_{i=1}^m \text{Tr}(E_i) \leq V. \end{aligned} \tag{5}$$

Similarly, a nested formulation of the minimum weight problem (4) is

$$\begin{aligned} & \underset{E \in \mathbb{E}}{\text{minimize}} && \sum_{i=1}^m \text{Tr}(E_i) \\ & \text{subject to} && \sum_{\ell \in L} w_\ell f_\ell^T A^{-1}(E) f_\ell \leq \gamma. \end{aligned} \tag{6}$$

In [29] it is shown that the function

$$c(E) = f_\ell^T A^{-1}(E) f_\ell$$

---

<sup>1</sup>This assumption is standard within structural optimization. In the implementation it is satisfied by forcing that  $E_i \succeq \varepsilon I$  for some small  $\varepsilon > 0$ .

is convex and infinitely continuously differentiable. Therefore, both problems (5) and (6) are convex SDPs since all other constraints are linear. Using the Schur complement theorem it can also be shown that problem (3) is equivalent to

$$\begin{aligned} & \underset{E \in \mathbb{E}, \varrho_\ell \geq 0}{\text{minimize}} && \sum_{\ell \in L} w_\ell \varrho_\ell \\ & \text{subject to} && \sum_{i=1}^m \text{Tr}(E_i) \leq V, \\ & && \begin{pmatrix} \varrho_\ell & f_\ell^T \\ f_\ell & A(E) \end{pmatrix} \succeq 0, \forall \ell \in L. \end{aligned} \quad (7)$$

Problem formulations similar to (7) have also been proposed for truss topology optimization in a number of articles, see e.g. [4, 5]. Problem (7) has a linear objective function, and linear vector and matrix inequalities. Hence, it is a linear SDP. For its linearity this formulation leads to a nice mathematical structure but with additionally very large-scale matrix inequalities which are difficult to deal with in computations, see e.g. [20]. For this reason problem (7) is excluded from our numerical experiment.

The minimum compliance problem (3) has the following dual formulation. For the derivation, please see the Appendix A.

$$\begin{aligned} & \underset{\substack{u_1, \dots, u_{n_\ell} \in \mathbb{R}^n \\ \alpha \in \mathbb{R}, \underline{\beta} \in \mathbb{R}^m, \bar{\beta} \in \mathbb{R}^m}}{\text{maximize}} && -\alpha \bar{V} + 2 \sum_{\ell \in L} w_\ell f_\ell^T u_\ell + \underline{\rho} \sum_{i=1}^m \underline{\beta}_i - \bar{\rho} \sum_{i=1}^m \bar{\beta}_i \\ & \text{subject to} && \sum_{\ell \in L} \sum_{k=1}^{n_G} w_\ell B_{i,k}^T u_\ell u_\ell^T B_{i,k} - (\alpha - \underline{\beta}_i + \bar{\beta}_i) I \preceq 0, i = 1, \dots, m \\ & && \alpha \geq 0, \bar{\beta} \geq 0, \underline{\beta} \geq 0. \end{aligned} \quad (8)$$

This is a problem with linear objective and convex quadratic constraints. Therefore, it is a convex problem. For this problem it can be verified that the Slater condition holds by choosing arbitrary  $u_\ell \in \mathbb{R}^n$ ,  $\underline{\beta} > 0$ ,  $\bar{\beta} > 0$ , and sufficiently large positive  $\alpha$ . Since problem (3) can also be equivalently written as convex problems, for example problem (5), the duality gap is zero. Similar results for min-max problems can also be found in [27] and [3]. A solution to the primal problem (3) can be obtained by solving the dual problem (8). The primal variable  $E$  appears in the primal-dual system of (8) as a Lagrangian multiplier to the matrix inequality constraints. It is thus important that the dual problem is solved up to optimality to get a structure supporting the external loads.

Throughout this article we use the following assumptions on the problem data in the FMO problems. Similar assumptions are stated, implicitly or explicitly, in e.g. [3].

A1 The loads are non-zero, i.e.  $f_\ell \neq 0$  for all  $\ell \in L$ .

A2 The trace bounds satisfy  $0 \leq \underline{\rho} < \bar{\rho} < +\infty$  and the volume bound satisfies

$$\sum_{i=1}^m \underline{\rho} < V < \sum_{i=1}^m \bar{\rho}.$$

A3 The stiffness matrix  $A(E)$  is positive definite for all  $E \succ 0$ .

A4 Given  $\gamma > 0$  and weights  $w_\ell > 0, \ell \in L$  there exists positive definite  $E \in \mathbb{E}$  such that  $\sum_{\ell \in L} w_\ell f_\ell^T A^{-1}(E) f_\ell \leq \gamma$ .

Assumption (A1) is to exclude trivial cases. Combining the positive definiteness of the stiffness matrix  $A(E)$  with assumption (A1) - (A4) imply that the feasible sets of problems (3), (4), and their equivalent problems are non-empty.

### 3 The primal-dual interior point method

In this section the primal-dual interior method is described in the setting of a general nonlinear SDP. The specializations to FMO problems are presented in Section 4. In line with the special structure of the FMO problems and motivated by the problem formulations in [29] we consider the nonlinear SDP

$$\begin{aligned} & \underset{X \in \mathbb{S}, u \in \mathbb{R}^n}{\text{minimize}} && f(X, u) \\ & \text{subject to} && g_j(X, u) \leq 0, \quad j = 1, \dots, k, \\ & && X_i \succeq 0, \quad i = 1, \dots, m, \end{aligned} \tag{9}$$

with

$$\mathbb{S} = \mathbb{S}^{d_1} \times \mathbb{S}^{d_2} \times \dots \times \mathbb{S}^{d_m} \text{ and } (d_1, d_2, \dots, d_m) \in \mathbb{N}^m.$$

The functions  $f, g_j : \mathbb{S} \times \mathbb{R}^n \rightarrow \mathbb{R}$ , for  $j = 1, \dots, k$  are assumed to be sufficiently smooth. After introducing slack variables  $s \in \mathbb{R}^k$  to problem (9) the associated barrier problem with barrier parameter  $\mu > 0$  is

$$\begin{aligned} & \underset{X \in \mathbb{S}_+, u \in \mathbb{R}^n, s \in \mathbb{R}_+^k}{\text{minimize}} && f(X, u) - \mu \sum_{i=1}^m \ln(\det(X_i)) - \mu \sum_{j=1}^k \ln(s_j) \\ & \text{subject to} && g_j(X, u) + s_j = 0, \quad j = 1, \dots, k. \end{aligned} \tag{10}$$

The central idea in interior point methods is that problem (10) is solved for a sequence of barrier parameter  $\mu_k$  approaching zero and the barrier problem

approaches the original problem (9). With Lagrangian multiplier  $\lambda \in \mathbb{R}_+^k$ , the Lagrangian to problem (10) is

$$\mathcal{L}_\mu(X, u, s, \lambda) = f(X, u) - \mu \sum_{i=1}^m \ln(\det(X_i)) - \mu \sum_{j=1}^k \ln(s_j) + \lambda^T (g(X, u) + s).$$

The first-order optimality conditions of the barrier problem (10) are

$$\nabla_X \mathcal{L}_\mu(X, u, s, \lambda) = \nabla_X f(X, u) - \mu X^{-1} + \nabla_X (g(X, u)^T \lambda) = 0 \quad (11a)$$

$$\nabla_u \mathcal{L}_\mu(X, u, s, \lambda) = \nabla_u f(X, u) + \nabla_u g(X, u)^T \lambda = 0 \quad (11b)$$

$$\nabla_s \mathcal{L}_\mu(X, u, s, \lambda) = -\mu S^{-1} e + \lambda = 0 \quad (11c)$$

together with the feasibility condition

$$g(X, u) + s = 0 \quad (12)$$

and positive definiteness of  $X$ , positivity of the slack variables  $s$  and the dual variables  $\lambda$ . Following standard techniques for interior point methods for linear SDP, see for example [22], we introduce the additional matrix variable  $Z$  satisfying

$$Z := \mu X^{-1} \quad (13)$$

in (11a) so that  $XZ - \mu I = 0$ . The optimality conditions in (11) are rewritten as

$$\begin{pmatrix} \nabla_X f(X, u) - Z + \nabla_X (g(X, u)^T \lambda) \\ \nabla_u f(X, u) + \nabla_u g(X, u)^T \lambda \\ S \Lambda e - \mu e \\ g(X, u) + s \\ XZ - \mu I \end{pmatrix} = \begin{pmatrix} 0 \\ 0 \\ 0 \\ 0 \\ 0 \end{pmatrix} \quad (14)$$

where  $S = \text{diag}(s)$ ,  $\Lambda = \text{diag}(\lambda)$ , and  $e = (1, 1, \dots, 1)^T$  is a vector of all ones of appropriate size.

It is important that symmetry is maintained during the linearization of the complementarity equation  $XZ - \mu I = 0$  in order to apply Newton's method to the system in (14). This can be achieved by using the linear operator  $H_P : \mathbb{R}^{n \times n} \rightarrow \mathbb{S}^n$ , introduced in [36], and defined by

$$H_P(Q) := \frac{1}{2} (PQP^{-1} + (PQP^{-1})^T)$$

where  $P \in \mathbb{R}^{n \times n}$  is some non-singular matrix. In [36], it is shown that

$$H_P(Q) = \mu I \Leftrightarrow Q = \mu I.$$

Therefore, the optimality conditions for (10) will be (14) with  $XZ = \mu I$  replaced by

$$H_P(XZ) = H_P(\mu I) = \mu I. \quad (15)$$

Applying Newton's method to the system in (14) gives the search direction

$$(\Delta X, \Delta u, \Delta s, \Delta \lambda, \Delta Z) \in \mathbb{S} \times \mathbb{R}^n \times \mathbb{R}^k \times \mathbb{R}^k \times \mathbb{S}$$

as the solution of the system

$$\begin{pmatrix} \nabla_{XX}^2 \mathcal{L}_\mu(X, u, s, \lambda) & \nabla_{Xu}^2 \mathcal{L}_\mu(X, u, s, \lambda)^T & 0 & \nabla_X g(X, u)^T & -I \\ \nabla_{Xu}^2 \mathcal{L}_\mu(X, u, s, \lambda) & \nabla_{uu}^2 \mathcal{L}_\mu(X, u, s, \lambda) & 0 & \nabla_u g(X, u)^T & 0 \\ 0 & 0 & \Lambda & S & 0 \\ \nabla_X g(X, u) & \nabla_u g(X, u) & I & 0 & 0 \\ \mathcal{E} & 0 & 0 & 0 & \mathcal{F} \end{pmatrix} \begin{pmatrix} \Delta X \\ \Delta u \\ \Delta s \\ \Delta \lambda \\ \Delta Z \end{pmatrix} = - \begin{pmatrix} \nabla_X f(X, u) - Z + \nabla_X (g(X, u)^T \lambda) \\ \nabla_u f(X, u) + \nabla_u g(X, u)^T \lambda \\ S\Lambda e - \mu e \\ g(X, u) + s \\ H_P(XZ) - \mu I \end{pmatrix}. \quad (16)$$

**Remark 3.1.** Some of the blocks in the coefficient matrix of the Newton's system (16) are tensors of order higher than two and the blocks in the right hand side and the search direction are combination of matrices and vectors. The violation of standard notation is intended to simplify the presentation. For the detailed meaning of the transposes and products, see Appendix B.

The block diagonal matrices  $\mathcal{E} = \mathcal{E}(X, Z)$  and  $\mathcal{F} = \mathcal{F}(X, Z)$  in (16) are the derivatives of  $H_P(XZ)$  with respect to  $X$  and  $Z$  respectively and are given by

$$\mathcal{E} = P \odot P^{-T} Z \text{ and } \mathcal{F} = PX \odot P^{-1} \quad (17)$$

where the operator  $P \odot Q : \mathbb{S}^n \rightarrow \mathbb{S}^n$  is defined by

$$(P \odot Q)K := \frac{1}{2}(PKQ^T + QKP^T).$$

By choosing among different matrices  $P$  in (17) we get different search directions. Directions obtained in this manner are called members of the Monteiro-Zhang (MZ) family [36]. In practice, the most used search directions are the AHO direction [2] obtained when  $P = I$ , the HRVW/KSH/M direction [16, 17, 21] when  $P = X^{-1/2}$ , the dual HRVW/KSH/M direction [17, 21] when  $P = Z^{1/2}$ , and the NT direction [23, 24] when  $P = W^{-1/2}$  with  $W = X^{1/2}(X^{1/2}ZX^{1/2})^{-1/2}X^{1/2}$ . For the case of FMO problems such as (3) and (8), the matrices  $\nabla_{XX}^2 \mathcal{L}_\mu(X, u, s, \lambda)$ ,

$\mathcal{E}$  and  $\mathcal{F}$  are block diagonal matrices where each block is small and relatively cheap to invert. Therefore, following the tradition in interior point methods for SDP, one can solve the reduced symmetric system

$$\begin{pmatrix} G & A \\ A^T & B \end{pmatrix} \begin{pmatrix} \Delta u \\ \Delta \lambda \end{pmatrix} = \begin{pmatrix} \tilde{r}_d \\ \tilde{r}_p \end{pmatrix} \quad (18)$$

where

$$\begin{aligned} G &= \nabla_{uu}^2 \mathcal{L}_\mu(X, u, s, \lambda) - \nabla_{Xu}^2 \mathcal{L}_\mu(X, u, s, \lambda) \tilde{H}^{-1} \nabla_{Xu}^2 \mathcal{L}_\mu(X, u, s, \lambda)^T \\ A &= \nabla_u g(X, u)^T - \nabla_{Xu}^2 \mathcal{L}_\mu(X, u, s, \lambda) \tilde{H}^{-1} \nabla_X g(X, u)^T \\ B &= -\Lambda^{-1} S - \nabla_X g(X, u) \tilde{H}^{-1} \nabla_X g(X, u)^T, \end{aligned}$$

and letting  $(R_d, r_d, r_c, r_p, R_C)^T$  denote the right hand side of the system (16)

$$\begin{aligned} \tilde{r}_d &= r_d - \nabla_{Xu}^2 \mathcal{L}_\mu(X, u, s, \lambda) \tilde{H}^{-1} (R_d + \mathcal{F}^{-1} R_C) \\ \tilde{r}_p &= r_p - \Lambda^{-1} r_c - \nabla_X g(X, u) \tilde{H}^{-1} (R_d + \mathcal{F}^{-1} R_C) \end{aligned}$$

with

$$\tilde{H} = \nabla_{XX}^2 \mathcal{L}_\mu(X, u, s, \lambda) + \mathcal{F}^{-1} \mathcal{E}.$$

The other search directions  $(\Delta X, \Delta s, \Delta Z)$  are then obtained from

$$\Delta X = \tilde{H}^{-1} (R_d + \mathcal{F}^{-1} R_C - \nabla_{Xu}^2 \mathcal{L}_\mu(X, u, s, \lambda)^T \Delta u - \nabla_X g(X, u)^T \Delta \lambda) \quad (19a)$$

$$\Delta Z = \mathcal{F}^{-1} (R_C - \mathcal{E} \Delta X) \quad (19b)$$

$$\Delta s = \Lambda^{-1} (r_c - S \Delta \lambda). \quad (19c)$$

Given a current iterate  $(X, u, s, \lambda, Z)$  and a search direction  $(\Delta X, \Delta u, \Delta s, \Delta \lambda, \Delta Z)$  the primal step length  $\alpha_p$  and dual step length  $\alpha_d$  are computed in two steps. First we compute the maximum possible step to the boundary of the feasible region by

$$\bar{\alpha}_p = \max\{\alpha \in (0, 1] : X + \alpha \Delta X \succeq (1 - \tau)X, s + \alpha \Delta s \geq (1 - \tau)s\} \quad (20a)$$

$$\bar{\alpha}_d = \max\{\alpha \in (0, 1] : Z + \alpha \Delta Z \succeq (1 - \tau)Z, \lambda + \alpha \Delta \lambda \geq (1 - \tau)\lambda\} \quad (20b)$$

where  $\tau \in (0, 1)$  is the fraction to the boundary parameter. Next, a backtracking line search can be performed to compute the final step lengths

$$\alpha_p \in (0, \bar{\alpha}_p], \text{ and } \alpha_d \in (0, \bar{\alpha}_d]$$

to get sufficient decrease in a merit function  $\phi$ . We use the norm of the optimality error given by

$$\begin{aligned} \phi_\mu(X, u, s, \lambda, Z) &:= \|\nabla_X f(X, u) - Z + \nabla_X (g(X, u)^T \lambda)\|_F^2 + \|(S\Lambda - \mu I)e\|_2^2 \\ &\quad + \|g(X, u) + s\|_2^2 + \|\nabla_u f(X, u) + \nabla_u g(X, u)^T \lambda\|_2^2 \\ &\quad + \|H_P(XZ) - \mu I\|_F^2 \end{aligned} \quad (21)$$

as merit function. A search direction is said to sufficiently decrease the merit function if

$$\begin{aligned} \phi_\mu(X + \alpha_p \Delta X, u + \alpha_p \Delta u, s + \alpha_p \Delta_d s, \lambda + \alpha_d \Delta \lambda, Z + \alpha_d \Delta Z) \\ \leq (1 - \tau_0 \eta) \phi_\mu(X, u, s, \lambda, Z) \end{aligned} \quad (22)$$

for a parameter  $\eta \in (0, 1)$  and for a constant  $\tau_0 \in (0, 1)$ . The new iterate  $(X^+, u^+, s^+, \lambda^+, Z^+)$  is then given by

$$(X^+, u^+, s^+) = (X, u, s) + \alpha_p (\Delta X, \Delta u, \Delta s) \quad (23a)$$

$$(\lambda^+, Z^+) = (\lambda, Z) + \alpha_d (\Delta \lambda, \Delta Z). \quad (23b)$$

The stopping criteria for the algorithm and the determination of the tolerances for the barrier problem (10) from the tolerances for the original problem (9) are motivated by [33]. Given that the optimality tolerance  $\epsilon^o > 0$  and the feasibility tolerance  $\epsilon^f > 0$  for the original problem (9) the interior point algorithm terminates when

$$\begin{aligned} \max \left\{ \max_i \|\nabla_{X_i} f(X, u) - Z_i + \nabla_{X_i} (g(X, u)^T \lambda)\|_F, \right. \\ \left. \|\nabla_u f(X, u) + \nabla_u g(X, u)^T \lambda\|_\infty \right\} \leq \epsilon^o \\ \max \{ \max_i \|H_P(X_i Z_i)\|_F, \|S \Lambda e\|_\infty \} \leq \epsilon^o \\ \|g(X, u)_+\|_\infty \leq \epsilon^f \end{aligned} \quad (24)$$

where  $g_j(X, u)_+ = \max\{0, g_j(X, u)\}$ . For the barrier problem (10) the tolerances are  $\mu$  dependent since barrier problems with large barrier parameter are not solved to optimality. The inner iteration of the interior point method stops when

$$\begin{aligned} \max \left\{ \max_i \|\nabla_{X_i} f(X, u) - Z_i + \nabla_{X_i} (g(X, u)^T \lambda)\|_F, \right. \\ \left. \|\nabla_u f(X, u) + \nabla_u g(X, u)^T \lambda\|_\infty \right\} \leq \epsilon_\mu^o \\ \max \{ \max_i \|H_P(X_i Z_i) - \mu I\|_F, \|S \Lambda e - \mu e\|_\infty \} \leq \epsilon_\mu^o \\ \|g(X, u) + S\|_\infty \leq \epsilon_\mu^f. \end{aligned} \quad (25)$$

In our numerical experiments we use

$$\epsilon_\mu^o = \max\{10\mu, \epsilon^o - \mu\} \quad \text{and} \quad \epsilon_\mu^f = \max\{10\mu, \epsilon^f\}. \quad (26)$$

It can be verified that determining the tolerances for the barrier problem as in (26) ensures that a point satisfying the inner stopping criteria for a small  $\mu$  value also satisfies the stopping criteria for the outer iteration.

We use two strategies to update the barrier parameter  $\mu$ . In the first strategy we estimate the  $\mu$  value from a given (not necessarily feasible) point  $(X, u, s, \lambda, Z)$ . By coupling results known from nonlinear programming and linear SDP,  $Tr(X^T Z) + s^T \lambda$  measures the gap between the objective functions of primal and dual problems. Therefore we estimate the current  $\mu$  value by

$$\mu = \sigma \left( \sum_i Tr(X_i^T Z_i) / d_i + s^T \lambda \right) / (m + k) \quad (27)$$

where  $\sigma < 1$  is a prescribed centring parameter. In our numerical experiment it is observed that this update strategy gives a monotone decrease in  $\mu$  for the problems we solve. The second strategy is a simple one. We initialize  $\mu$  value and update it as

$$\mu^+ = \varepsilon_0 \mu, \quad \text{for } \varepsilon_0 < 1. \quad (28)$$

The over all description of the interior point method is given in Algorithm 1.

**Remark 3.2.** Our primary focus is to develop efficient methods for FMO problems. Since the FMO formulations in Section 2 such as (3) and (8) are all well-posed we do not include any techniques to detect infeasibility or unboundedness in the description of the primal-dual interior point method in Algorithm 1.

## 4 Algorithmic details for FMO problems

In this section we discuss the optimality conditions and the primal-dual systems for the interior point method specialized to the different FMO problem formulations in Section 2. The discussion in the rest of this section is for a single load case problem to simplify notations. The subscript  $\ell$  in  $u_\ell$  and  $f_\ell$  is also dropped. Furthermore, we introduce the operators  $\mathcal{T}_1 : \mathbb{S} \rightarrow \mathbb{R}^m$  defined by  $(\mathcal{T}_1 E)_i = Tr(E_i)$  and  $\mathcal{T}_2 : \mathbb{S} \rightarrow \mathbb{R}$  defined by  $\mathcal{T}_2 E = \sum_i Tr(E_i)$  for every  $E = (E_1, \dots, E_m)^T \in \mathbb{S}$ . The adjoints of these operators are  $\mathcal{T}_1^* : \mathbb{R}^m \rightarrow \mathbb{S}$  defined by  $(\mathcal{T}_1^* y)_i = y_i I$  for every  $y \in \mathbb{R}^m$  and  $\mathcal{T}_2^* : \mathbb{R} \rightarrow \mathbb{S}$  defined by  $(\mathcal{T}_2^* \alpha)_i = \alpha I$  for every  $\alpha \in \mathbb{R}$  where the identity matrix  $I$  in both cases has the same size as  $E_i$ .

Introducing the slack variables  $(\bar{r}, \underline{r}, s) \in \mathbb{R}_+^m \times \mathbb{R}_+^m \times \mathbb{R}_+$  to the minimum

---

**Algorithm 1** A primal-dual interior point algorithm for nonlinear SDP problems.

---

Choose  $w_p^0 = (X^0, u^0, s^0)$ ,  $w_d^0 = (\lambda, Z)$ , and  $(\mu_0$  or use (27)).  
Set the outer iteration counter  $k \leftarrow 0$ .  
**while** stopping criteria (24) for problem (9) is not satisfied and  $k < \hat{k}_{max}$  **do**  
  Set the inner iteration counter  $i \leftarrow 0$   
  **while** stopping criteria (25) for problem (10) is not satisfied and  $i < i_{max}$   
  **do**  
    Compute the search direction  $\Delta w_p^{k,i}$  and  $\Delta w_d^{k,i}$  by solving system (18) and (19).  
    Compute  $\bar{\alpha}_p$  and  $\bar{\alpha}_d$  as in (20).  
    Set the line search iteration counter  $l \leftarrow 0$ .  
    Set **LineSearch**  $\leftarrow$  **False**  
    **while** **LineSearch** = **False** and  $l < l_{max}$  **do**  
       $\alpha_p \leftarrow \eta^l \bar{\alpha}_p$  and  $\alpha_d \leftarrow \eta^l \bar{\alpha}_d$   
      **if**  $\phi_\mu(w_p^{k,i} + \alpha_p \Delta w_p^{k,i}, w_d^{k,i} + \alpha_d \Delta w_d^{k,i}) \leq (1 - \tau_0 \eta^l) \phi_\mu(w_p^{k,i}, w_d^{k,i})$  **then**  
        Set the new iterate  $(w_p^{k,i+1}, w_d^{k,i+1})$  as in (23).  
        **LineSearch**  $\leftarrow$  **True**  
      **else**  
         $l \leftarrow l + 1$ .  
      **end if**  
    **end while**  
     $i \leftarrow i + 1$ .  
  **end while**  
  Update  $\mu_{k+1}$  as in (27) or (28).  
   $k \leftarrow k + 1$ .  
**end while**

---

compliance problem (3), the associated barrier problem is given by

$$\begin{aligned}
& \underset{u \in \mathbb{R}^n, E \in \mathbb{E}, \bar{r}, \underline{r}, s}{\text{minimize}} && f^T u - \mu \sum_{i=1}^m \ln(\det(E_i)) - \mu \sum_{i=1}^m \ln(\bar{r}_i) - \mu \sum_{i=1}^m \ln(\underline{r}_i) - \mu \ln(s) \\
& \text{subject to} && A(E)u - f = 0, \\
& && \mathcal{T}_1 E + \bar{r} - \bar{\rho} e = 0, \\
& && \rho e - \mathcal{T}_1 E + \underline{r} = 0, \\
& && \mathcal{T}_2 E + s - V = 0,
\end{aligned} \tag{29}$$

where  $\mu > 0$  is barrier parameter. The slack variables are implicitly kept strictly

positive. Then problem (29) has the following Lagrange function

$$\begin{aligned} \mathcal{L}(x) = & f^T u - \mu \sum_{i=1}^m \ln(\det(E_i)) - \mu \sum_{i=1}^m \ln(\bar{r}_i) - \mu \sum_{i=1}^m \ln(\underline{r}_i) - \mu \ln(s) \\ & + \lambda^T (A(E)u - f) + \bar{\beta}^T (\mathcal{T}_1 E + \bar{r} - \bar{\rho}e) \\ & + \underline{\beta}^T (\underline{\rho}e - \mathcal{T}_1 E + \underline{r}) + \alpha (\mathcal{T}_2 E + s - V), \end{aligned} \quad (30)$$

where  $x = (E, u, \bar{r}, \underline{r}, s, \lambda, \bar{\beta}, \underline{\beta}, \alpha)$  with  $(\lambda, \bar{\beta}, \underline{\beta}, \alpha) \in \mathbb{R}^n \times \mathbb{R}_+^m \times \mathbb{R}_+^m \times \mathbb{R}_+$  Lagrange multipliers. With the technique in (13) the optimality conditions to problem (29) are

$$\lambda^T F(u) - Z + \mathcal{T}_1^* \bar{\beta} - \mathcal{T}_1^* \underline{\beta} + \mathcal{T}_2^* \alpha = 0 \quad (31a)$$

$$A(E)\lambda + f = 0 \quad (31b)$$

$$A(E)u - f = 0 \quad (31c)$$

$$\mathcal{T}_1 E + \bar{r} - \bar{\rho}e = 0 \quad (31d)$$

$$\underline{\rho}e - \mathcal{T}_1 E + \underline{r} = 0 \quad (31e)$$

$$\mathcal{T}_2 E + s - V = 0 \quad (31f)$$

$$\bar{R}\bar{B} - \mu e = 0 \quad (31g)$$

$$\underline{R}\underline{B} - \mu e = 0 \quad (31h)$$

$$s\alpha - \mu = 0 \quad (31i)$$

$$H_P(E, Z) - \mu I = 0 \quad (31j)$$

where

$$\bar{B} = \text{diag}(\bar{\beta}), \underline{B} = \text{diag}(\underline{\beta}), \bar{R} = \text{diag}(\bar{r}), \underline{R} = \text{diag}(\underline{r}),$$

and  $F(u) = (A_1(E)^{j,k}u, \dots, A_m(E)^{j,k}u)$  with  $A_i(E)^{j,k} = \frac{\partial A_i(E)}{\partial (E_i)^{j,k}}$  and the multiplication  $\lambda^T F(u)$  defined such that  $(\lambda^T F(u))_i = \lambda^T A_i(E)^{j,k}u$  for each  $j$  and  $k$  in the set of indices of  $E_i$ . Under the assumption  $E_i \succ 0$  for all  $i$ , the matrix  $A(E)$  is positive definite. Therefore, the equation  $A(E)\lambda + f = 0$  uniquely determines the Lagrange multiplier  $\lambda$ . By setting  $\lambda = -u$  we get a reduced set of optimality conditions consisting of the primal residuals (31c)-(31f), the perturbed complementary conditions (31g)-(31j) and

$$-u^T F(u) - Z + \mathcal{T}_1^* \bar{\beta} - \mathcal{T}_1^* \underline{\beta} + \mathcal{T}_2^* \alpha = 0. \quad (32)$$

We denote by  $R_d$  the negative of the left hand sides of (32), by  $(r_{p_1}, \dots, r_{p_4})$  the negative of the primal residuals and by  $(r_{c_1}, \dots, r_{c_3}, R_{c_4})$  the negative of perturbed complementary residuals. Applying Newton's method to the reduced

system and eliminating the search directions  $\Delta\bar{\beta}$ ,  $\Delta\underline{\beta}$ ,  $\Delta\bar{r}$ ,  $\Delta\underline{r}$ , and  $\Delta s$  as in (36) results in the saddle point system

$$\begin{pmatrix} -\frac{1}{2}A(E) & F(u) & 0 \\ \bar{F}(u)^T & D & \mathcal{T}_2^* \\ 0 & \mathcal{T}_2 & -s/\alpha \end{pmatrix} \begin{pmatrix} \Delta\tilde{u} \\ \Delta E \\ \Delta\alpha \end{pmatrix} = \begin{pmatrix} f - A(E)u \\ R_1 \\ r_1 \end{pmatrix} \quad (33)$$

where the block diagonal matrix  $D$  is given by

$$D = \mathcal{F}^{-1}\mathcal{E} + \mathcal{T}_1^*(\bar{R}^{-1}\bar{B} + \underline{R}^{-1}\underline{B})\mathcal{T}_1.$$

Note that  $F(u)\Delta E = \sum_i \sum_{j,k} (A_i(E)^{j,k}u)(\Delta E_i)_{j,k}$  with  $j$  and  $k$  in the set of indices of  $E_i$ .

The residuals  $R_1$  and  $r_1$  are given by

$$R_1 = R_d + \mathcal{F}^{-1}R_{c_4} - \mathcal{T}_1^*\bar{R}^{-1}(r_{c_1} - \bar{B}r_{p_2}) + \mathcal{T}_1^*\underline{R}^{-1}(r_{c_2} - \underline{B}r_{p_3}) \quad (34)$$

$$r_1 = r_{p_4} - \frac{1}{\alpha}r_{c_3}. \quad (35)$$

The other search directions are then computed as

$$\Delta u = -\Delta\tilde{u} \quad (36a)$$

$$\Delta Z = \mathcal{F}^{-1}(R_{c_4} - \Delta E) \quad (36b)$$

$$\Delta\bar{r} = r_{p_2} - \mathcal{T}_1\Delta E \quad (36c)$$

$$\Delta\underline{r} = r_{p_3} + \mathcal{T}_1\Delta E \quad (36d)$$

$$\Delta\bar{\beta} = \bar{R}^{-1}(r_{c_1} + \bar{B}(-r_{p_2} + \mathcal{T}_1\Delta E)) \quad (36e)$$

$$\Delta\underline{\beta} = \underline{R}^{-1}(r_{c_2} + \underline{B}(-r_{p_3} - \mathcal{T}_1\Delta E)) \quad (36f)$$

$$\Delta s = \frac{1}{\alpha}(r_{c_3} - s\Delta\alpha). \quad (36g)$$

The change of variables in (36a) is introduced to make the coefficient matrix in the saddle point system (33) symmetric. Next we present the saddle point system to the nested minimum compliance problem (5). The compliance  $c(E) = f^T A^{-1}(E)f$  has the completely dense Hessian

$$\nabla^2 c(E) = 2F(u(E))^T A^{-1}(E)F(u(E)), \text{ where } u(E) = A^{-1}(E)f \quad (37)$$

see e.g. [29]. Following a similar procedure as above, problem (5) results in the saddle point system

$$\begin{pmatrix} 2F(u(E))^T A^{-1}(E)F(u(E)) + D & \mathcal{T}_2^* \\ \mathcal{T}_2 & -s/\alpha \end{pmatrix} \begin{pmatrix} \Delta E \\ \Delta\alpha \end{pmatrix} = \begin{pmatrix} R_1 \\ r_1 \end{pmatrix}. \quad (38)$$

We can formulate an equivalent but sparse system to (38). We introduce a dummy variable  $\Delta\tilde{u}$  such that

$$2A^{-1}(E)F(u(E))\Delta E = \Delta\tilde{u}$$

and get a larger but sparse system

$$\begin{pmatrix} -\frac{1}{2}A(E) & F(u(E)) & 0 \\ F(u(E))^T & D & \mathcal{T}_2^* \\ 0 & \mathcal{T}_2 & -s/\alpha \end{pmatrix} \begin{pmatrix} \Delta\tilde{u} \\ \Delta E \\ \Delta\alpha \end{pmatrix} = \begin{pmatrix} 0 \\ R_1 \\ r_1 \end{pmatrix}. \quad (39)$$

In FMO problems the systems (38) and (33) are large-scale due to the large size of the design variable  $E$  and the number of degrees of freedom. Since each block matrices in the block diagonal matrix  $D$  is also relatively small and cheap to invert we further eliminate  $\Delta E$  from the systems and solve a smaller system with coefficient matrix

$$\begin{pmatrix} -\frac{1}{2}A(E) - F(u)D^{-1}F(u)^T & -F(u)D^{-1}\mathcal{T}_2^* \\ -\mathcal{T}_2D^{-1}F(u)^T & -s/\alpha - \mathcal{T}_2D^{-1}\mathcal{T}_2^* \end{pmatrix} \quad (40)$$

in the variables  $(\Delta\tilde{u}, \Delta\alpha)$  and with updated right hand side. Our numerical experiments show that for larger problems it is even more efficient to eliminate again  $\Delta\alpha$  from (40) and solve the system with coefficient matrix

$$-\frac{1}{2}A(E) - F(u)D^{-1}F(u)^T - F(u)D^{-1}\mathcal{T}_2^*(-s/\alpha - \mathcal{T}_2D^{-1}\mathcal{T}_2^*)^{-1}(\mathcal{T}_2D^{-1}F(u)^T) \quad (41)$$

in  $\Delta\tilde{u}$  and then use the Sherman-Morrison formula [14] in which we only factorize the sparse matrix

$$-\frac{1}{2}A(E) - F(u)D^{-1}F(u)^T. \quad (42)$$

**Remark 4.1.** The reduction of the system by setting  $\lambda$  to some scalar multiple of  $u$  is limited to the classical FMO problems considered in this article. This reduction may not be possible if other problem formulations are considered, for example, problems that include local stress constraints, see [19].

**Remark 4.2.** The difference in sparsity pattern of the matrices  $A(E)$  and  $F(u)D^{-1}F(u)^T$  is more visible for multiple load problems with the second matrix being much more dense than the first matrix.

**Remark 4.3.** For problems (4), (6), and (8) similar saddle point systems to either (33) or (39) in size and structure can be formulated.

**Remark 4.4.** For the minimum weight problem in the simultaneous analysis and design approach (4) we set  $\lambda = -\alpha u$ , where  $\lambda$  and  $\alpha$  are Lagrange multipliers, to the elastic equilibrium equation  $A(E)u - f = 0$  and to  $f^T u + s - \gamma = 0$  respectively to get reduced optimality conditions.

**Remark 4.5.** Since the matrix variables  $(E, Z)$  and hence the search directions  $(\Delta E, \Delta Z)$  are symmetric, the computations are performed with the entries only in the lower triangular parts of these matrices.

## 5 Implementation, algorithmic parameters, and problem data

The interior point method and the finite element routines are implemented entirely in MATLAB Version 7.7 (R2008b). All numerical experiments are run on Intel Xeon X5650 six-core CPUs running at 2.66 GHz with 4GB of memory per core (only a single core is used per problem). The finite elements used are standard four node bilinear elements obtained by full Gaussian integration, see e.g. [9].

The saddle point systems (40) and (42) and the elastic equilibrium equation in the case of the nested problem formulations (5) and (6) are solved using the  $LU$  factorization routines which are built into MATLAB. As described in Section 3 different choices of the matrix  $P$  in (17) result in different search directions. Table 1 shows how the block diagonal matrices  $\mathcal{E}$ ,  $\mathcal{F}$ , and the right hand side  $R_{c_4}$  of the linearised equation of the complementarity equation (31j) for the AHO, the HRVW/KSV/M and the NT directions are computed. Computation of the NT direction follows from [31]. The matrix  $G$  in Table 1 is determined by first performing a Cholesky factorization on  $E$  and  $Z$ , namely,

$$E = LL^T \text{ and } Z = RR^T$$

and then singular value decomposition on  $R^T L$ , say  $UDV^T = R^T L$ . Then we have

$$G = LVD^{-1/2}.$$

Table 1: Computation of  $\mathcal{E}$ ,  $\mathcal{F}$  and the right hand side  $R_{c_4}$ .

	AHO ( $P = I$ )	HRVW/KSV/M ( $P = Z^{1/2}$ ) and pre- and post- multiplying by $Z^{-1/2}$	NT ( $P = W^{-1/2}$ $= G^{-1}$ )
$\mathcal{E}$	$I \odot Z$	$I \odot I$	$G^{-1} \odot G^T Z$
$\mathcal{F}$	$E \odot I$	$E \odot Z^{-1}$	$G^{-1} E \odot G^T$
$R_{c_4}$	$\sigma\mu I - \frac{1}{2}(EZ + ZE)$	$\sigma\mu Z^{-1} - E$	$\sigma\mu - D^2$

The optimality tolerance is set to  $\epsilon^o = 10^{-7}$  while the feasibility tolerance is  $\epsilon^f = 10^{-8}$  for all problems. The optimality and feasibility tolerances for the

barrier problems are computed as in (26). We say that the current iterate is a solution if it satisfies the stopping criteria for the inner and outer iterations as outlined in (25) and (24). The minimum barrier parameter value  $\mu_{\min}$  is set to  $10^{-9}$ . The boundary to the fraction parameter  $\tau$  is set to 0.9. The parameters used in the backtracking line search are set as  $\eta = 0.5$  and  $\tau_0 = 10^{-5}$ , respectively. For all problems we observe that the algorithm converges without performing any line search. This could be because the treated problems are either convex or can be equivalently written as a convex problem. For this reason the line search part of the algorithm was not activated in the numerical experiments. Both barrier update strategies given in (27) and (28) are implemented. In the numerical experiments we use (27) with  $\sigma = 0.4$  since the  $\mu$  values in this case are proportional to the duality gap.

The primal design variables are initially set to  $E_i = 0.1\bar{\rho}I$  for all  $i$ , while the primal displacement variables are set to zero, i.e.  $u_\ell = 0$  for all  $\ell$ . All slack variables are all set to ones and that Lagrange multipliers for equality constraints are set to zero. Lagrange multipliers for scalar (or matrix) inequalities are otherwise set to ones (or identity matrices). When solving minimum compliance problems the total weight fraction is set to 33.3% of the maximum weight, i.e.  $V = (m/3)\bar{\rho}$ . When solving the minimum weight problems the bound on the compliance is set to 25% of the compliance evaluated at the initial point. The local bounds on the  $Tr(E_i)$  are scaled in such away that  $\bar{\rho}/\underline{\rho} = 10^4$ .

## 6 Numerical experiments

The numerical experiments have three objectives. The first goal is to compare the performance of the interior point method when applied to the different FMO formulations presented in Section 2 and determine the best choice of formulation. The second goal is to investigate the numerical behaviour of the AHO, the HRVW/KSV/M, and the NT search directions and give recommendations. We use performance profiles as introduced in [10] to evaluate the numerical performances. The number of iterations and CPU time of the method required to obtain a solution are used as measures of the performances. The third goal is to show the efficiency of the method. This is achieved first by reporting solutions to a set of large-scale FMO problems. Second, by solving benchmark problems and making comparison to the recent numerical results presented in [29]. The results in [29] are obtained using a state-of-the-art special purpose method for FMO problems.

Throughout the article we use the colour bar in Figure 1 to show the optimal density distribution, that is, the trace of the stiffness tensor of the optimal designs.



Figure 1: Colour bar for the optimal density distribution.

## 6.1 Performance

We consider a set of FMO problem instances over 2D design domains to compare the performance of the formulations and search directions. Four two-dimensional benchmark problems from [37], [7], and [19] are considered. The design domains, boundary conditions, and loads for these problems are shown in Figure 2. The first one is a single load Cantilever beam problem with design domain dimensions  $2 \times 1$ . The second problem is a single load Michell beam problem with design domain dimensions  $2 \times 1$ . In the third problem we consider an L-shaped design domain with dimension  $1 \times 1$  with a quarter square removed from one corner. The last benchmark is a two load problem with a rectangular design domain of dimension  $2 \times 1$ . In all cases we apply a load over a segment of length 0.04. For each design domain there are four level of finite element discretizations with the finer mesh obtained from the coarser by refining each element into four elements. Details of the problem instances are given in Table 2.

### 6.1.1 Performance of the formulations

Considering the minimum compliance problem we solve the three formulations, namely, the simultaneous analysis and design approach (3), the dual formulation (8), and the nested approach (5) for all problem instances in Table 2. It is shown in Figure 5 that the performance profiles are similar. The identical profiles of the dual and SAND formulations in Figure 5a is the result of the similarity (up to a scaling) of the optimality conditions (once  $\lambda$  is eliminated from the optimality condition of the SAND formulation to get (32)). While solving the nested formulation the additional computational effort of solving the elastic equilibrium equations as in the second part of (37) at each interior point iteration is almost not visible in the performance profiles. It is slightly more noticeable for the multiple load case problems. For example, for solving the minimum weight problem on the "Two Loads Case IV" in Table 2, the average CPU time spent on one interior point iteration was 453 seconds for solving the problem of SAND formulation and 465 seconds for the problem of nest formulation. We expect higher computational efforts if we solve much larger problems or problems over 3D design domains. For the minimum weight problem we solve the simultaneous

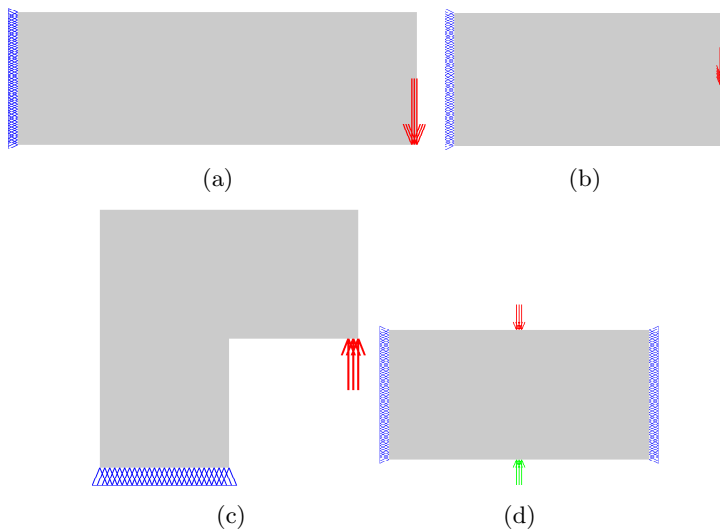


Figure 2: Design domains, boundary conditions, and external loads for the Cantilever benchmark problem (a), the Michell beam problem (b), the L-shape problem (c), and the two load case problem (d).

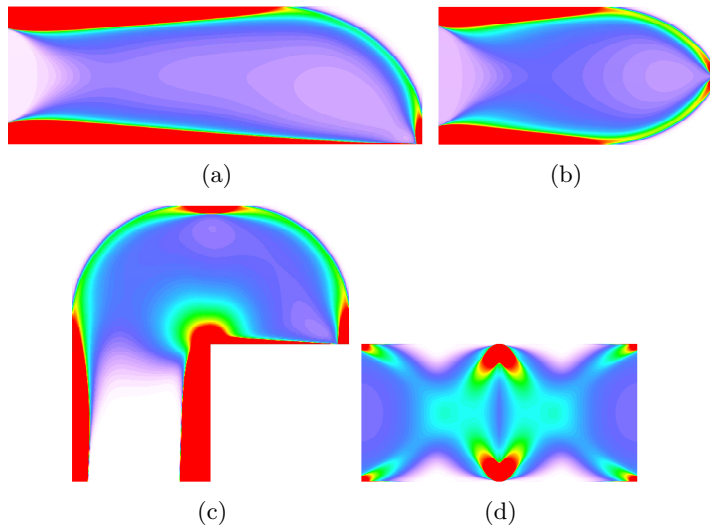


Figure 3: Optimal density distribution obtained by solving the minimum compliance problem (3) for the Cantilever IV benchmark problem (a), the Michell IV beam problem (b), the L-shape IV problem (c), and the two load case IV problem (d).

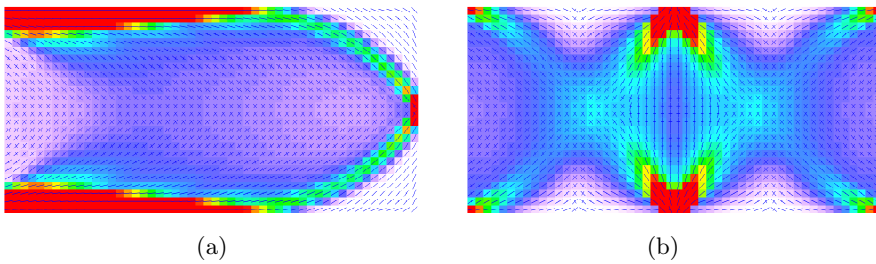


Figure 4: Principal material directions for the optimal designs for the Michell beam problem (a), and the two load case problem (b).

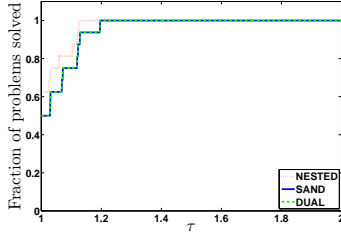
Table 2: Problem instances.

Problems	No. of finite elements	No. of design variables	No. of non-fixed state variables
Cantilever I	7500	45000	15300
Cantilever II	30000	180000	60600
Cantilever III	120000	720000	241200
Cantilever IV	480000	2880000	962400
Michell I	5000	30000	10200
Michell II	20000	120000	40400
Michell III	80000	480000	160800
Michell IV	320000	1920000	641600
L-shape I	1875	11250	3900
L-shape II	7500	45000	15300
L-shape III	30000	180000	60600
L-shape IV	120000	720000	241200
Two Loads case I	5000	30000	10098
Two Loads case II	20000	120000	40198
Two Loads case III	80000	480000	160398
Two Loads case IV	320000	1920000	640798

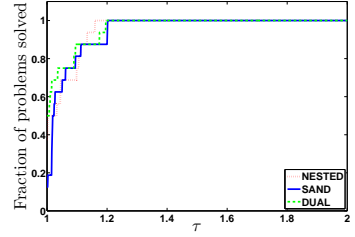
analysis and design problem (4) and the nested formulation (6) for all problem instances in Table 2. Figure 6 suggests similar results as to the minimum weight problems.

### 6.1.2 Performance of the search directions

We compare the numerical performance of the AHO, the HRVW/KSV/M, and the NT search directions. We solve the problem formulation in (3) for all problem instances in Table 2 using all search directions. Figure 7a shows that the number of iterations is fewer when using the AHO and NT directions compared to the HRVW/KSV/M direction. In our numerical experiments we generally get larger optimality error in each first inner iteration for HRVW/KSV/M direction than for the other two directions. As a result the method requires more inner iterations per outer iteration when the HRVW/KSV/M direction is used. It seems that this issue can be resolved by choosing a more aggressive barrier update strategy, for example, as in (28) with  $\varepsilon_0 = 0.1$ . However, this results in numerical instabilities for some of the problems as the iterates are close to the optimal solution. We also experience that the AHO direction is more sensitive than the NT direction to changes in algorithmic parameters and barrier update strategies. The plot in Figure 7b suggests that the CPU time for using the NT direction is in between the

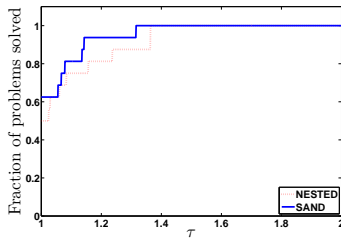


(a)

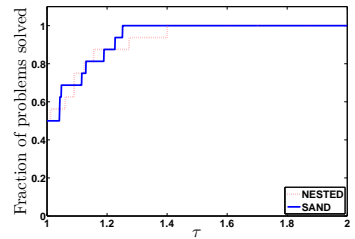


(b)

Figure 5: Performance profiles for the formulations of the minimum compliance problem. Number of iterations as performance measure (a), CPU time as performance measure (b).



(a)



(b)

Figure 6: Performance profiles for the formulations of the minimum weight problem. Number of iterations as performance measure (a), CPU time as performance measure (b).

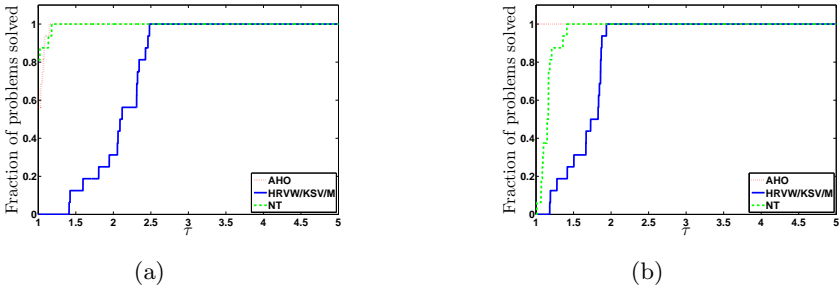


Figure 7: Performance profiles for the search directions. Number of iterations as performance measure (a), CPU time as performance measure (b).

AHO and the HRVW/KSV/M directions. This is because we perform Cholesky factorizations of each  $E_i$  and  $Z_i$  for  $i = 1, \dots, m$  and the additionally the Singular Value Decompositions of a matrix computed from the Cholesky factorizations.

The plots for the optimal density distribution of each design domain is given in Figure 3. The principal material directions of optimal designs for the Michell beam and the two load case problems are shown in Figure 4. The directions are computed based on the principal eigenvectors associated to the Voigt-stiffness tensor. The numerical result for solving problem (3) for each problem instances in Table 2 is given in Table 3.

## 6.2 Efficiency compared to alternative methods

The problems listed in Table 3 are, by far, the largest FMO problems reported to date. The proposed primal-dual interior point method requires a modest number of iterations. All problem instances reported in Table 3 are solved within 25-55 iterations. Table 3 illustrates that there is a mild increase in number of iterations with increasing problem size. We also notice that when solving the largest problems the memory requirements and the computational expense of the method are largely dominated by the solution of the saddle point system (42) and additionally of the elastic equilibrium equation for the nested formulations.

We also make comparisons with the FMO results presented in [29]. The problems in [29] are solved by the code PENSCLP. At present the comparison is limited only to problems considered in this article. The comparison is indeed merely in a sense that we solve a multiple load case of problem formulation (5) while in [29] an alternative worst-case multiple problem is solved. Moreover, the loading and the size of fixed boundary regions could differ up to scaling. Comparison on CPU time also have discrepancy for the fact that the programming languages

Table 3: Numerical results for the problem instances in Table 2 and the minimum compliance problem (3).

Problems	No. of iterations	CPU time (s)	Compliance
Cantilever I	34	213	5.0816
Cantilever II	44	1128	5.0802
Cantilever III	40	4257	5.0826
Cantilever IV	40	17713	5.0925
Michell I	34	142	1.8331
Michell II	48	819	1.8349
Michell III	55	3809	1.8362
Michell IV	49	13787	1.8391
L-shape I	29	47	2.1780
L-shape II	35	215	2.1814
L-shape III	35	896	2.1845
L-shape IV	34	3518	2.1885
Two Loads case I	25	134	0.4220
Two Loads case II	28	622	0.4253
Two Loads case III	30	2941	0.4263
Two Loads case IV	31	14441	0.4272

and the machines used to perform numerical experiments are different. However, the reported results are still interesting since the efficiency both in CPU time and number of iterations required to get even a higher quality solution is significant. The design domain, boundary conditions, and loads are depicted in Figure 8. In Table 4 we report the numerical results for a four load case with three different discretizations. In the first column we list the number of finite elements, in the second column the number of iterations, in the third column the achieved optimality and feasibility tolerances, and in the fourth column the CPU time. In the fifth and sixth columns we include the number of iterations and the CPU time from [29] required by PENSOP to solve the problem. Note that the CPU times reported include the entire computation process, i.e, starting from mesh and finite element generations to the end of the optimization process. When we compare the obtained results to the results in Table 7.1 in [29], we notice that the efficiency of the proposed interior point method both in time and number of iteration. The solutions obtained with the interior point method are also more accurate. In [29] one of the stopping criteria used is a measure of the optimality error that is set to lower tolerance than used in our numerical experiment. We also solve another problem with 5000 elements for three different load cases. The numerical result is presented in Table 5. In this table the first column contains the load cases and the other columns are similar to those of Table 4. This table

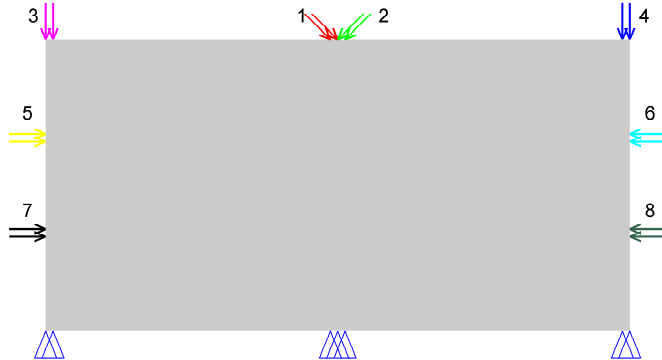


Figure 8: Design domain, boundary conditions, and external loads for the problem instances listed in Tables 4 and 5.

also shows the efficiency of the interior point method and accuracy of solutions when we compare to the results in Table 7.2 in [29].

We are also able to obtain a solution for 80000 finite elements and 8 load cases within 36 iterations and 81420 seconds. The optimal design is shown in Figure 9b.

Table 4: Numerical results for solving problem (5) with 4 load case. The two last columns in the table are from [29].

FEs	iter	opt/feas	CPU time <sub>(s)</sub>	iter PENSCP	CPU time (s), PENSCP
1250	26	0.0000e+00/6.7531e-08	56	622	256
5000	27	0.0000e+00/6.0402e-08	254	482	1027
20000	29	0.0000e+00/5.3046e-08	1298	522	7878

## 7 Conclusions

We propose an efficient primal-dual interior point method for several classical formulations of FMO. The number of iterations the method requires is appealing and increases only slowly with increases in problem size. With the interior point method we solve, by far, the largest FMO problem reported to date. The

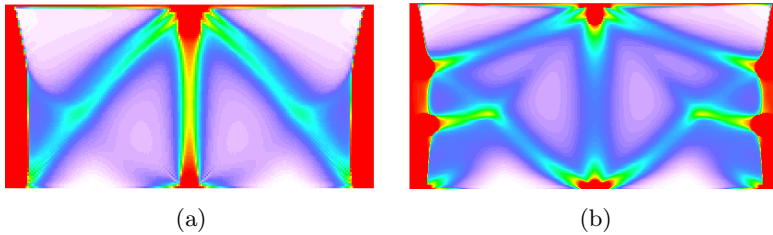


Figure 9: Optimal density distribution for the multiple load problem in Figure 8. Problem with 20000 finite elements and 4 load cases as described in Tables 4 and 5 (a), problem with 80000 finite elements and 8 load cases (b).

Table 5: Numerical results for solving problem (5). The design domain is partitioned into 5000 finite elements. The two last columns in the table are from [29].

Lc	iter	opt/feas	CPU time (s)	iter PENSCP	CPU time (s) PENSCP
2	31	0.0000e+00/1.2200e-08	166	543	585
4	27	0.0000e+00/6.0402e-08	245	489	1027
8	28	0.0000e+00/2.7303e-08	738	370	1319

obtained accuracy of the computed optimal solutions is higher compared to solutions obtained by other methods developed for FMO. For large-scale problems the memory requirements and the computation time of the method are dominated by the direct solution of the saddle point systems for computing the search direction. Future research will be directed towards developments of efficient preconditioner for iterative methods for the saddle-point systems with the aim to solve very large-scale 3D problems.

The number of iterations of the method is similar when solving either of the simultaneous analysis and design or the nested problem formulations. For solving the nested problem formulation the additional expected computational effort of solving the elastic equilibrium equations at each interior point iteration is almost not visible for the problems sizes considered. However, the differences that can be seen when solving multiple load problems could indicate higher computational efforts if we solve much larger problems or problems over 3D design domains. The dual formulation (8) also works well. However, there are no dual reformulations like (8) if other constraints, such as stress constraints, are included in the problem

formulations.

Our numerical experiments indicate that the NT and AHO directions are more efficient than the HRVW/KSV/M direction as they require fewer inner iterations per outer iteration. Comparing the AHO and NT directions we experience that the NT directions are less sensitive to changes in algorithmic parameters and speed of updating the barrier parameter. Therefore, the NT direction is our preferred choice.

The results in this article are exclusively supported by numerical experiments. Theoretical treatment of convergence theory of the interior point method must be further analysed. The applicability of relevant available theories in the literature should be investigated and potentially applied to show global convergence.

## 8 Acknowledgements

The authors would like to thank two reviewers for their constructive and insightful comments and suggestions. We also would like to express our gratitude to our former colleague Stefanie Gaile for many and fruitful discussions on Free Material Optimization.

The research was partially funded by the Danish Council for Strategic Research through the *Danish Center for Composite Structures and Materials* (DCCSM).

## References

- [1] Achtziger, W., Bendsøe, M., Ben-Tal, A., Zowe, J.: Equivalent displacement based formulations for maximum strength truss topology design. *Impact of Computing in Science and Engineering* **4**, 315–345 (1992)
- [2] Alizadeh, F., Haeberly, J., Overton, M.: Primal-dual interior-point methods for semidefinite programming: convergence rates, stability and numerical results. *SIAM Journal on Optimization* **8**(3), 746–768 (2009)
- [3] Ben-Tal, A., Kočvara, M., Nemirovski, A., Zowe, J.: Free material design via semidefinite programming: The multiload case with contact conditions. *SIAM Journal on Optimization* **9**(4), 813–832 (1999)
- [4] Ben-Tal, A., Nemirovski, A.: Robust truss topology design via semidefinite programming. *SIAM Journal on Optimization* **7**(4), 991–1016 (1997)
- [5] Ben-Tal, A., Nemirovski, A.: *Handbook of semidefinite programming*, chap. Structural Design, pp. 443–467. Kluwer Academic Publishers (2000)

- [6] Bendsøe, M., Díaz, A.: Optimization of material properties for Mindlin plate design. *Structural Optimization* **6**, 268–270 (1993)
- [7] Bendsøe, M., Guedes, J., Haber, R., Pedersen, P., Taylor, J.: An analytical model to predict optimal material properties in the context of optimal structural design. *Journal of Applied Mechanics* **61**, 930–937 (1994)
- [8] Benson, H., Shanno, D.: Interior-point methods for nonconvex nonlinear programming: regularization and warmstarts. *Computational Optimization and Applications* **40**, 143–189 (2008)
- [9] Cook, R., Malkus, D., Plesha, M., Witt, R.: *Concepts and Applications of Finite Element Analysis*, 4th edn. John Wiley and Sons (2002)
- [10] Dolan, E., Moré, J.: Benchmarking optimization software with performance profiles. *Mathematical Programming* **97**(A), 201–213 (2002)
- [11] Forsgren, A., Gill, P.: Primal-dual interior methods for nonconvex nonlinear programming. *SIAM Journal on Optimization* **8**(4), 1132–1152 (1998)
- [12] Forsgren, A., Gill, P., Wright, M.: Interior methods for nonlinear optimization. *SIAM Review* **44**(4), 525–597 (2002)
- [13] Gaile, S.: Free material optimization for shells and plates. Ph.D. thesis, Institute of Applied Mathematics II, Friedrich-Alexander University of Erlangen-Nuremberg (2011)
- [14] Golub, G., van Loan, C.: *Matrix Computations*, 3rd edn. Johns Hopkins University Press (1996)
- [15] Haslinger, J., Kočvara, M., Leugering, G., Stingl, M.: Multidisciplinary free material optimization. *SIAM Journal on Applied Mathematics* **70**(7), 2709–2728 (2010)
- [16] Helmberg, C., Rendl, F., Vanderbei, R., Wolkowicz, H.: An interior-point method for semidefinite programming. *SIAM Journal on Optimization* **6**, 342–361 (1996)
- [17] Kojima, M., Shindoh, S., Hara, S.: Interior-point methods for the monotone semidefinite linear complementarity problem in symmetric matrices. *SIAM Journal on Optimization* **7**(1), 86–125 (1997)
- [18] Kočvara, M., Stingl, M.: PENNON A code for convex nonlinear and semidefinite programming. *Optimization Methods and Software* **18**(3), 317–333 (2003)

- [19] Kočvara, M., Stingl, M.: Free material optimization for stress constraints. *Structural and Multidisciplinary Optimization* **33**, 323–335 (2007)
- [20] Kočvara, M., Stingl, M., Zowe, J.: Free material optimization: recent progress. *Optimization* **57**(1), 79–100 (2008)
- [21] Monteiro, R.: Primal-dual path-following algorithms for semidefinite programming. *SIAM Journal on Optimization* **7**(3), 663–678 (1997)
- [22] Monteiro, R.: First- and second-order methods for semidefinite programming. *Mathematical Programming* **97**, 209–244 (2003)
- [23] Nesterov, Y., Todd, M.: Self-scaled barriers and interior-point methods for convex programming. *Mathematics of Operations Research* **22**(1), 1–42 (1997)
- [24] Nesterov, Y., Todd, M.: Primal-dual interior-point methods for self-scaled cones. *SIAM Journal on Optimization* **8**(2), 324–364 (1998)
- [25] Ringertz, U.: On finding the optimal distribution of material properties. *Structural Optimization* **5**, 265–267 (1993)
- [26] Stingl, M.: On the solution of nonlinear semidefinite programs by augmented Lagrangian method. Ph.D. thesis, Institute of Applied Mathematics II, Friedrich-Alexander University of Erlangen-Nuremberg (2006)
- [27] Stingl, M., Kočvara, M., Leugering, G.: Free material optimization with fundamental eigenfrequency constraints. *SIAM Journal on Optimization* **20**(1), 524–547 (2009)
- [28] Stingl, M., Kočvara, M., Leugering, G.: A new non-linear semidefinite programming algorithm with an application to multidisciplinary free material optimization. *International Series of Numerical Mathematics* **158**, 275–295 (2009)
- [29] Stingl, M., Kočvara, M., Leugering, G.: A sequential convex semidefinite programming algorithm with an application to multiple-load free material optimization. *SIAM Journal on Optimization* **20**(1), 130–155 (2009)
- [30] Todd, M.: A study of search directions in primal-dual interior-point methods for semidefinite programming. *Optimization Methods and Software* **11**, 1–46 (1999)
- [31] Todd, Y., Toh, K., Tütüncü, R.: On the Nesterov-Todd direction in semidefinite programming. *SIAM Journal on Optimization* **8**(3), 769–796 (1998)

- [32] Vogelbusch, C.H.: Numerical treatment of nonlinear semidefinite programs. Ph.D. thesis, Institut für Mathematik der Heinrich-Heine-Universität Düsseldorf (2006)
- [33] Waltz, R., Morales, J., Nocedal, J., Orban, D.: An interior algorithm for nonlinear optimization that combines line search and trust region steps. *Mathematical Programming* **107**, 391–408 (2006)
- [34] Werner, R.: Free material optimization-mathematical analysis and numerical solution. Ph.D. thesis, Institute of Applied Mathematics II, Friedrich-Alexander University of Erlangen-Nuremberg (2001)
- [35] Yamashita, H., Yabe, H., Harada, K.: A primal-dual interior point method for nonlinear semidefinite programming. *Mathematical Programming* **135**, 89–121 (2012)
- [36] Zhang, Y.: On extending some primal-dual interior-point algorithms from linear programming to semidefinite programming. *SIAM Journal on Optimization* **8**(2), 365–386 (1998)
- [37] Zowe, J., Kočvara, M., Bendsøe, M.: Free material optimization via mathematical programming. *Mathematical Programming* **79**, 445–466 (1997)

## Appendix A

In this Appendix we derive the dual formulation (8) of the minimum weighted compliance problem (3). Similar result for minimax problems can be found in [3]. Analogous all-quadratic formulations of minimum compliance truss topology optimization problems are described, for example, in [1]. The linear elasticity static structural analysis problem can be written as

$$\sup_{u_\ell} \{2f_\ell^T u_\ell - u_\ell^T A(E)u_\ell\}$$

which is a quadratic problem with negative definite Hessian and hence a concave maximization problem. The optimality condition is  $A(E)u_\ell = f_\ell$  and the optimal value is  $f_\ell^T u_\ell$  if  $f_\ell \in \mathcal{R}(A(E))$  and  $-\infty$  otherwise. Due to the stated assumptions we replace the sup with max in the following. Therefore, the minimum compliance

problem (3) is equivalent to

$$\begin{aligned}
& \underset{E_1, \dots, E_m \succeq 0}{\text{minimize}} && \sum_{\ell \in L} w_\ell \max_{u_\ell} \{2f_\ell^T u_\ell - u_\ell^T A(E) u_\ell\} \\
& \text{subject to} && \rho \leq \text{Tr}(E_i) \leq \bar{\rho}, i = 1, \dots, m, \\
& && \sum_{i=1}^m \text{Tr}(E_i) \leq \bar{V}.
\end{aligned} \tag{43}$$

The Lagrangian  $\mathcal{L}$  associated with (43) is

$$\begin{aligned}
\mathcal{L}(E, u_\ell, \alpha, \bar{\beta}, \underline{\beta}) &= \sum_{\ell \in L} w_\ell \max_{u_\ell} \{2f_\ell^T u_\ell - u_\ell^T A(E) u_\ell\} + \sum_{i=1}^m \underline{\beta}_i (-\text{Tr}(E_i) + \rho) \\
&+ \sum_{i=1}^m \bar{\beta}_i (\text{Tr}(E_i) - \bar{\rho}) + \alpha (\sum_{i=1}^m \text{Tr}(E_i) - \bar{V}) \\
&= \max_{u_1, \dots, u_{n_L}} \sum_{\ell \in L} w_\ell (2f_\ell^T u_\ell - u_\ell^T A(E) u_\ell) + \sum_{i=1}^m \underline{\beta}_i (-\text{Tr}(E_i) + \rho) \\
&+ \sum_{i=1}^m \bar{\beta}_i (\text{Tr}(E_i) - \bar{\rho}) + \alpha (\sum_{i=1}^m \text{Tr}(E_i) - \bar{V}) \\
&= \max_{u_1, \dots, u_{n_L}} \left( \sum_{\ell \in L} w_\ell (2f_\ell^T u_\ell - u_\ell^T A(E) u_\ell) + \sum_{i=1}^m \underline{\beta}_i (-\text{Tr}(E_i) + \rho) \right. \\
&+ \left. \sum_{i=1}^m \bar{\beta}_i (\text{Tr}(E_i) - \bar{\rho}) + \alpha (\sum_{i=1}^m \text{Tr}(E_i) - \bar{V}) \right) \\
&= \max_{u_1, \dots, u_{n_L}} \left( \sum_{\ell \in L} 2w_\ell f_\ell^T u_\ell - \alpha \bar{V} + \rho \sum_{i=1}^m \underline{\beta}_i - \bar{\rho} \sum_{i=1}^m \bar{\beta}_i \right. \\
&+ \left. \sum_{i=1}^m \left\langle E_i, (\alpha - \underline{\beta}_i + \bar{\beta}_i) I - \sum_{\ell \in L} \sum_{k=1}^{n_G} w_\ell B_{i,k}^T u_\ell u_\ell^T B_{i,k} \right\rangle \right).
\end{aligned}$$

The corresponding dual function is

$$\begin{aligned}
& g(u_1, \dots, u_{n_L}, \underline{\beta}, \bar{\beta}, \alpha) \\
&= \underset{E_1, \dots, E_m \succeq 0}{\text{minimize}} \quad \max_{u_1, \dots, u_{n_L}} \left( \sum_{\ell \in L} 2w_\ell f_\ell^T u_\ell - \alpha \bar{V} + \rho \sum_{i=1}^m \underline{\beta}_i - \bar{\rho} \sum_{i=1}^m \bar{\beta}_i \right. \\
&\quad \left. + \sum_{i=1}^m \left\langle E_i, (\alpha - \underline{\beta}_i + \bar{\beta}_i) I - \sum_{\ell \in L} \sum_{k=1}^{n_G} w_\ell B_{i,k}^T u_\ell u_\ell^T B_{i,k} \right\rangle \right) \\
&= \begin{cases} \max_{u_1, \dots, u_{n_L}} \left( \sum_{\ell \in L} 2w_\ell f_\ell^T u_\ell - \alpha \bar{V} + \rho \sum_{i=1}^m \underline{\beta}_i - \bar{\rho} \sum_{i=1}^m \bar{\beta}_i \right) & \text{if (44) holds} \\ -\infty & \text{otherwise.} \end{cases}
\end{aligned}$$

Below is the condition that the dual function  $g$  attains its minimum value.

$$\sum_{\ell \in L} \sum_{k=1}^{n_G} w_\ell B_{i,k}^T u_\ell u_\ell^T B_{i,k} \preceq (\alpha - \underline{\beta}_i + \bar{\beta}_i) I, \quad i = 1, \dots, m. \quad (44)$$

The dual formulation of the minimum compliance problem (3) becomes

$$\begin{aligned}
& \sup_{u_1, \dots, u_{n_L}, \alpha \geq 0, \bar{\beta} \geq 0, \underline{\beta} \geq 0} \quad -\alpha \bar{V} + 2 \sum_{\ell \in L} w_\ell f_\ell^T u_\ell + \rho \sum_{i=1}^m \underline{\beta}_i - \bar{\rho} \sum_{i=1}^m \bar{\beta}_i \\
& \text{subject to} \quad \sum_{\ell \in L} \sum_{k=1}^{n_G} w_\ell B_{i,k}^T u_\ell u_\ell^T B_{i,k} - (\alpha - \underline{\beta}_i + \bar{\beta}_i) I \preceq 0, \quad i = 1, \dots, m.
\end{aligned}$$

## Appendix B

The following products are in tensor notation.

1.  $(\nabla_{X_r X_s}^2 \mathcal{L}_\mu(X, u, s, \lambda) \Delta X_s)_{ij} = (\nabla_{X_r X_s}^2 \mathcal{L}_\mu(X, u, s, \lambda))_{ijpq} (\Delta X_s)_{pq}$ , for  $r, s = 1, \dots, m$ , for  $i, j = 1, \dots, d_r$ , and for  $p, q = 1, \dots, d_s$ .
2.  $(\nabla_{X_r u}^2 \mathcal{L}_\mu(X, u, s, \lambda) \Delta X_r)_i = (\nabla_{u X_r}^2 \mathcal{L}_\mu(X, u, s, \lambda))_{ipq} (\Delta X_r)_{pq}$ , for  $r = 1, \dots, m$ , for  $p, q = 1, \dots, d_r$ , and for  $i = 1, \dots, n$ .
3.  $(\nabla_{X_r u}^2 \mathcal{L}_\mu(X, u, s, \lambda)^T \Delta u)_{ij} = (\nabla_{X_r u}^2 \mathcal{L}_\mu(X, u, s, \lambda))_{ijp} (\Delta u)_p$ , for  $r = 1, \dots, m$ , for  $i, j = 1, \dots, d_r$ , and for  $p = 1, \dots, n$ .
4.  $(\nabla_{X_r} g(X, u)^T \Delta \lambda)_{ij} = (\nabla_{X_r} (g(X, u)^T \Delta \lambda))_{ij}$ , for  $r = 1, \dots, m$ , and for  $i, j = 1, \dots, d_r$ .
5.  $(\nabla_{X_r} g(X, u) \Delta X_r)_i = (\nabla_{X_r} g_i(X, u))_{pq} (\Delta X_r)_{pq}$ , for  $r = 1, \dots, m$ , for  $p, q = 1, \dots, d_r$ , and for  $i = 1, \dots, k$ .